STELLARATORS

D.A. Hartmann

Max-Planck Institut für Plasmaphysik, EURATOM Association
Wendelsteinstrasse 1
17491 Greifswald
Tel. (49) 3834882478, Fax (49) 3834882509

ABSTRACT

Stellarators are toroidal devices where the required rotational transform of the magnetic field lines is generated by external field coils and not via an induced net toroidal plasma current. This confinement scheme has the advantages that, in principle, steady-state plasma operation is possible and that it does not have to brace itself against disruptions of a toroidal plasma current. At the cost of having to give up toroidal symmetry the properties of the stellarator field can be tailored to suit reactor needs. Research focuses on the plasma confinement properties of different stellarator fields and investigates the problems arising when one extrapolates to reactor parameters

I. INTRODUCTION

In a toroidal device the magnetic field lines need to be helically twisted in order to prevent polarisation of the plasma by drifting particles and thus to provide plasma confinement [1]. In addition, during many toroidal revolutions the field lines need to trace out surfaces, the so called flux surfaces. Figure 1 shows a toroidal section of four nested flux surfaces with one magnetic field line highlighted. Such nested flux surfaces can be created (mainly) in two ways: In a tokamak a toroidal field is superposed with the poloidal field of a net toroidal current induced in the plasma. In a stellarator[1] the net toroidal current is zero and the confining magnetic field is generated solely by external field coils. This requires some of the coils to helically revolve around the plasma.

The goal of stellarator research - as well as tokamak research - is to prove that the concept is suitable for a fusion reactor. Thus it is necessary to determine the magnetic field structure that can confine a plasma at sufficiently high density, n, and temperature, T, with sufficiently long energy confinement time, τ_E, in order to meet the Lawson criterion [2].

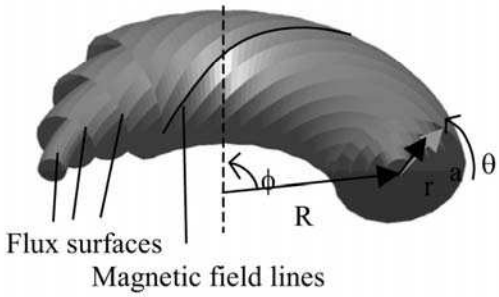

Figure 1 Nested flux surfaces ergodically covered by helical field lines.

In Table 1 the highest plasma parameters achieved in tokamaks and helical systems are summarised. Particularly the maximum central ion and electron temperatures of helical systems are lagging behind those of tokamaks and on first glance it is not obvious why this concept is still being pursued. According to present understanding, however, the differences are largely due to the different sizes of the present day experiments and not due to an inherent shortcoming of the stellarator concept.

	Tokamaks	Helical systems
$T_i(0)$ [keV]	44	4
$T_e(0)$ [keV]	15	7
$n_e(0)$ [$10^{20}m^{-3}$]	10	7
τ_E [s]	1	0.15
τ_{plasma} [s]	120	90
$<\beta>$ [%]	12.3	2.9
P_{fusion} [MW]	17	-

Table 1 Maximal plasma parameters achieved in tokamaks and stellarators in different discharges.

Larger experiments are being developed because of the attractiveness of the concept: The stellarator field can be stationary thus steady-state operation with plasma is possible rather than a pulsed operation as may be necessary in tokamaks. This reduces material fatigue due to thermal cycles in a reactor and avoids the requirement to store thermal loads. Also (as will be seen in subsequent lectures) the net toroidal plasma current in a tokamak constitutes a large reservoir of free energy that can quickly be released

[1] In this lecture the term "stellarator" is used in a generic sense for helical confinement systems encompassing traditional stellarators, helias stellarators, torsatrons, heliotrons, and heliacs. These terms will be explained further down.

in sudden disruptions. This causes severe strain on the mechanical structure and since stellarators do not have a net toroidal current the engineering requirements can be relaxed. In addition, tokamak research of the last decade has shown that the energy confinement time, the maximum plasma pressure and the highest density all are proportional to the plasma current. Thus tokamaks are required to operate at higher plasma currents in order to obtain better plasma performance.

During the 1950s research on controlled thermonuclear fusion was classified until it became clear near the end of that decade that progress was arduous and required international collaboration rather than secrecy. Historically, one of the first toroidal magnetic confinement experiment was the model "C" stellarator built by the astrophysicist Lyman Spitzer [2] in the fifties. However, at the IAEA meeting in 1968 the Russian tokamak T-3 showed confinement times which where thirty-fold higher than the stellarator values. This led to a surge towards new tokamak experiments; for example, the C stellarator was converted into the ST tokamak. Stellarator research, on the other hand, was continued at four laboratories in Germany, United Kingdom, U.S.A. and Japan only. Since then the stellarator concept has undergone many changes and the original short-comings are understood. Whereas the size of the tokamaks steadily increased, stellarators did not keep up with them. Only the latest experiments: the Large Helical Device (LHD) in Japan (R=3.9 m, operational since 1998, [3]) and Wendelstein 7-X in Germany (R=5.5m, operation planned for 2012, [5]) will have plasma volumes comparable with medium size tokamaks. Both have super-conducting coils and will investigate near steady-state plasma discharges with a duration of 30 minutes. In addition, some smaller experiments, e.g. Quasi-helically Symmetric Experiment, HSX, (R=1.2m, operation since 2000, [6]) and the National Compact Stellarator Experiment, NCSX, (R=1.2m, operation planned for 2009) pursue the study of optimising the magnetic field with respect to different aspects of particle kinetics or the influence of the plasma on the confining magnetic field.

This paper gives a brief overview of some aspects of stellarator research. Section II classifies the multitude of possibilities of using external coils to generate a toroidal, helical field. Section III describes the properties of the vacuum magnetic field of helical devices. When a plasma is generated in a helical device, plasma currents flow that lead to a deviation of the magnetic field from the vacuum magnetic field. This is the subject of Section IV. Section V relates plasma confinement to the magnetic field properties. Section VI shows how neo-classical transport in a helical devices can be reduced by a radial electric field to such an extend that the stellarator concept becomes viable for a fusion reactor. Section VII summarizes stellarator research that is directly reactor relevant: high plasma β, long pulse operation, particle exhaust with helical and island divertors. Finally, Section XIII gives an overview of the problems that are the focus of current stellarator research.

II. STELLARATOR GENEOLOGY

The stellarator magnetic field is generated by a suitable assembly of external field coils only. Since there is no net toroidal current one obtains for the poloidal component of the magnetic field: $\int B_\theta(r) r d\theta = 0$. Besides having twisted magnetic field lines, it is also necessary for plasma confinement that the field lines trace out nested magnetic flux surfaces [1]. There is no general analytic proof that a stellarator field has nested flux surfaces. However, one can numerically trace the field lines and investigate whether such surfaces exist. If they do exist one can show that they cannot be toroidally symmetric. Thus whereas for an ideal tokamak field, $B = B(r,\theta)$, for the stellarator field $B = B(r,\theta,\varphi)$. At first glance this seems to be a disadvantage since this entails that the generalised momentum, p_φ, is not a separable quantity, i.e. is not conserved as it is in a tokamak. This has profound consequences on transport in a stellarator. However, this freedom can also be put to one's advantage and allows to tailor the magnetic field to the specific needs of a fusion reactor. This is done in most of the recent stellarator experiments.

There is a plethora of ways of how to externally produce a helical field [6]. They can be divided into two groups: In the first group the magnetic field is generated by an assembly of field coils of simple geometric forms, e.g. planar, helical. These devices require at least one coil to encircle the torus toroidally. The nomenclature of these helical devices is given by the number of helical coils and the direction of the current flowing in them. The second group are devices where the magnetic field is generated by modular field coils of complicated geometric shape that encircle the torus only poloidally. Optimising the properties of the magnetic field of helical devices became possible only after magnetic field coils were no longer required to be of simple geometric shape. These devices are labelled according to the principal optimisation criteria.

A classical stellarator consists of a set of planar field coils that generate a toroidal magnetic field and a set of *l* dipole coils that are wound around the torus circumference *n* times. Wendelstein 7-A (Germany) [8] was such a *l=2, n=5* classical stellarator and is shown in Figure 2. The direction of the current in the helical coils is indicated. The currents in neighbouring coils flow in opposite directions. The last closed flux surface clearly shows the three-dimensional structure of the plasma. The plasma cross section is approximately elliptical and rotates with increasing toroidal angle.

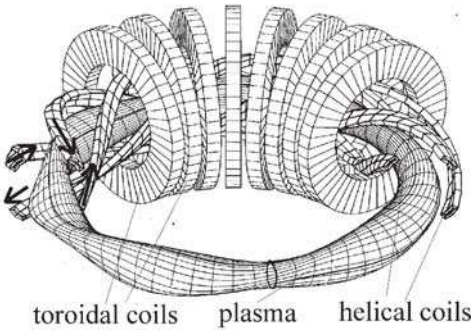

Figure 2. Cut open schematic of the l=2, n=5-stellarator W7-A.

Helical magnetic field lines and nested flux surfaces can also be obtained if the currents in the helical coils all flow into the same direction; then the toroidal field component does not cancel and it is even possible to dispose of the toroidal field coils all together (lest one wants to retain them for some additional experimental freedom). Such a device is called a torsatron (heliotron in Japanese literature). In such a situation also the average vertical magnetic field does not vanish and it is necessary to add an additional vertical field (generated by horizontal coils) in order to form a magnetic axis. The advanced toroidal facility (ATF, U.S.A.) was a l=2, n=6 torsatron [9]. It is schematically shown in Figure 3.

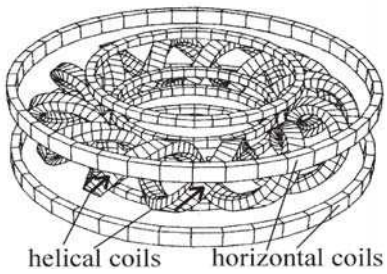

Figure 3 Coil system of the l=2, n=6 torsatron ATF.

In a heliac, finally, the centers of the toroidal field coils are no longer in one plane but follow a helical line. TJ-II [10] (Spain, operative since 1997) is an example and shown in Figure 4. There a horizontal coil for an additional vertical field has been added to increase the flexibility of the magnetic field configuration.

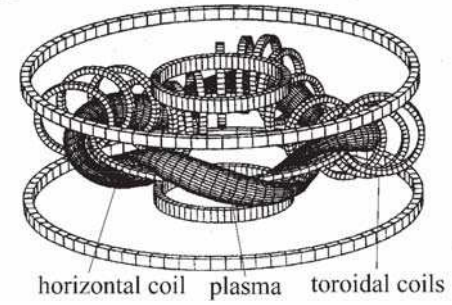

Figure 4 Schematic of the heliac TJ-II.

It is also possible to use non-planar coils altogether. Here one starts out with a magnetic field of desired properties and uses the fact that the magnetic field on a enclosing surface uniquely determines the magnetic field within. This magnetic field can be generated by a current distribution on another enclosing shell [11]. The current distribution might be continuous but one can approximate it with a set of discrete paths of constant current. These discrete paths define the coils. After calculating the magnetic field generated by the coils and comparing it with the desired field one can derive a set of coils in an iterative process.

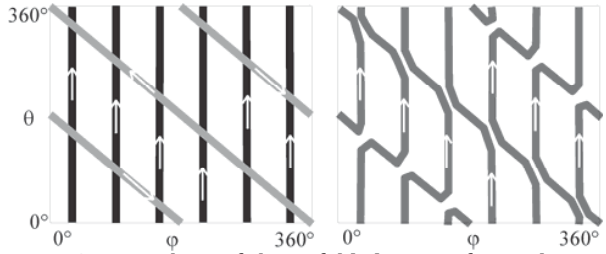

Figure 5 Current sheet of the unfolded torus of n=1, l=1 stellarator (left) and its equivalent set of modular coils. (right).

This procedure is illustrated in Figure 5 for the case of a standard l=1, n=1-stellarator where the set of toroidal and helical coils is replaced by a set of modular coils that generate approximately the same magnetic field. Figure 5 left shows the currents in the toroidal and helical coils on the torus surface that has been projected into the φ,θ-plane. If the currents in the toroidal and helical coils are equal then rearranging the current paths is possible. In Figure 5 right the new set of current paths is shown. Note that all of them are linked only poloidally and the currents do not intersect with one another. Thus the magnetic field coils are modular.

Wendelstein 7-AS was the first stellarator that used such a modular coil system. The set of coils is shown in Figure 6. The additional toroidal coils are used to increase the experimental variability but are not essential. The magnetic field is based on the field of a *l=2,n=5*-stellatator. The *n=5* structure was retained such that the magnetic field has a five-fold symmetry, i.e. the magnetic field is invariant under rotation around the z-axis by 360°/5=72°. The freedom gained by giving up the need to use coils of simple geometric shapes was used to optimize the magnetic field. Here, the magnetic field is similar to five magnetic mirrors that form the edges of a pentagon. Regions of high magnetic curvature, thus poor confinement, are located at the mirror ends with higher magnetic field, thus fewer particles. Other helical devices with modular coils are HSX with a magnetic field that is quasi-helical, W7-X optimized for reduced Shafranov shift and the formerly planned but since abandoned experiment QPS in the U.S.A. [12] with a quasi-poloidal field.

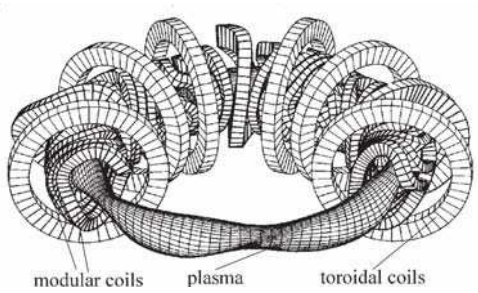

Figure 6 Schematic of the modular stellarator W7-AS.

III. VACUUM MAGNETIC FIELD

The vacuum magnetic is characterised by the poloidal cross-section of the flux surfaces, including magnetic islands, mod B contours, profile of the rotational transform ι the magnetic well and particles orbits in the vacuum magnetic field.

The cross-section of the magnetic field in one poloidal plane can be obtained by tracing field lines and plotting their intersection with one poloidal plane, similar to Poincaré plots in real space. The surface of a magnetic flux tube is identified as the line that is traced out by the intersection points of one field line during many revolutions around the torus. Using different starting positions for the field line tracing yields different flux surfaces. These results can be compared with measurements done with an electron beam generated by an electron gun inside of the evacuated vacuum region. The beam electrons follow the magnetic field line at the location of the gun and circle around the torus several times until they are observed by an intersecting scintillating grid [13] or by a moving scintillating rod in one poloidal plane [13,15]. Moving the location of the beam gun to a different starting point in the poloidal plane one obtains the location of different flux surfaces. Figure 7 shows the measured and calculated flux surfaces on LHD.

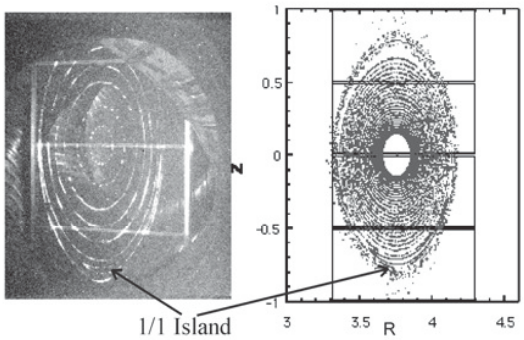

Figure 7 Measured (left) and calculated (right) flux surfaces of LHD.

One can identify three different regions: An inner region where the field lines form closed nested flux surfaces. This region can be perturbed by magnetic islands [16] that are caused by magnetic field errors. In Figure 7 an island is indicated that was caused by a field error that has a dominant *n=1, l=1* component. This region can be surrounded by an additional region of islands that are caused by the toroidicity of the field and are not necessarily due to field errors, i.e. they would not occur in a linear device. Therefore they are also referred to as "natural islands". Between the islands and the nested flux surfaces one can identify X- and O-points similar to the field of a divertor tokamak. Taking advantage of them one expects to be able to apply the successful concepts of a divertor in tokamaks also to stellarators [17]. Outside of the islands the field lines become stochastic with short connection lengths to the torus walls. Even though the flux surfaces have a complicated three-dimensional structure fast equilibrium processes along the field lines assure that they are also surfaces of constant plasma pressure. They can be ordered by assigning each surface the effective radius, r_{eff}, of a torus with cylindrical cross-section and the same major radius, R, that contains the same volume. The average twist of the magnetic field lines on a given flux surface is described by the rotational transform, ι, given by

$$\iota(r_{\text{eff}}) = \frac{R \cdot \langle B_\theta \rangle}{r_{\text{eff}} \cdot \langle B_\varphi \rangle} \equiv \frac{2\pi}{q(r_{\text{eff}})}$$

which is proportional to the inverse of the safety factor, q. Geometrically, this is the number of toroidal rotations that are necessary for one poloidal rotation. Historically, tokamaks use the safety factor q and stellarators use the rotation . In Figure 8 the rotational transform profiles are shown for different stellarators and compared with a tokamak. In a tokamak the toroidal plasma current and therefore the contribution to the poloidal magnetic field decreases with distance from the center; thus the rotation decreases. In a stellarator field the poloidal field increases with distance from the center because the contribution of the (outside) helical coils increases.

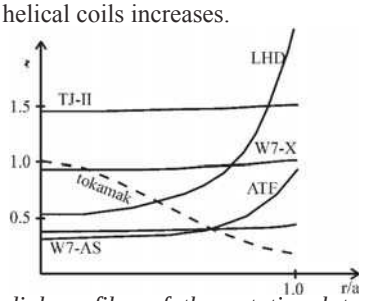

Figure 8 Radial profiles of the rotational transform of different helical devices and comparison with the tokamak profile.

Magnetic shear, $S = d\iota/dr$, describes the radial variation of the rotation. It is obvious from Figure 8 that stellarators and tokamaks have opposite sign of the shear and it is interesting to note that tokamak discharges with "reversed shear" that often have improved plasma confinement properties, locally have the same sign as a stellarator. If the ι profile is flat the pitch angle of the magnetic field on neighbouring flux surfaces changes. W7-AS and W7-X are examples for that. LHD (as all torsatrons) is an experiment with strong shear.

Devices with strong shear inevitably have flux surfaces with rotational transform $\iota = m/n$, with m and n

small natural numbers, so called "rational surfaces". There local instabilities can develop that locally destroy these flux surfaces by island formation which themselves short-circuit the inner plasma core to the plasma boundary thus degrading the plasma confinement. As shown in Figure 7 field errors, b_{per}, of a particular toroidal and poloidal mode structure can also resonate with the corresponding rational flux surface and cause the formation of islands. The width of the islands W becomes smaller with increased shear, $W \approx \sqrt{b_{per}/S}$ [16]. Thus strong shear is favourable for plasma confinement. On the other hand in devices with nearly vanishing shear, it is possible to avoid low order rational surfaces all together by properly choosing the rotational transform at the edge. This also has beneficial effects on confinement (see Section IV).

It is instructive to unwrap a flux surface and plot the contours of the constant total magnetic field versus toroidal angle, φ, and poloidal angle, θ. θ=0 denotes the outside horizontal midplane. Figure 9 shows mod $\underline{B}$ plots of an ideal tokamak and of the stellarator W7-AS. The solid line marks one representative field line as it wraps around the torus. An ideal tokamak (with infinitely many toroidal field coils, a finite number of coils causes an additional small ripple) is toroidally symmetric and the highest field is on the inboard side, $\theta = 180°$, the lowest on the outboard side, $\theta = 0°$. In a stellarator this toroidal symmetry is broken by the helical field coils leading to an additional fine structure of magnetic hills and valleys. The additional variation of the magnetic field along a field line is called magnetic ripple.

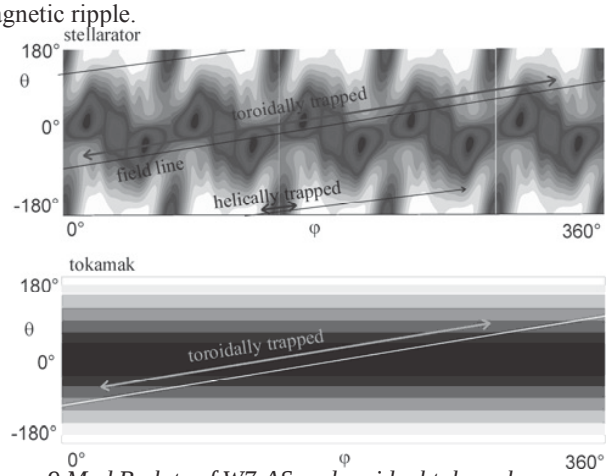

Figure 9 Mod B plots of W7-AS and an ideal tokamak.

As has been pointed out before [17] the undulating magnetic field leads to different classes of particle motion. In a tokamak there exist passing particles that approximately follow the magnetic field lines (and rotate toroidally) and toroidally trapped particles that are bouncing back and forth between the high magnetic field on the inside of the torus as indicated in Figure 9. In a stellarator there is an additional class of particles that are trapped in the local magnetic mirrors of the helical field. They are also shown in Figure 9.

The curvature and $\underline{\nabla B}$-drift [16] cause deviation of the particle orbits from the flux surface that is particularly pronounced for trapped particles. Figure 10 shows the traces of the three classes of particle motion projected into a poloidal plane of magnetic co-ordinates for W7-AS. The circles indicate magnetic flux surfaces. The high field side is on the left. Passing particles have orbits that stay close to the magnetic flux surface. Toroidally trapped particles have orbits of the familiar banana-shape. Helically trapped particles are trapped in a small poloidal range and often have a superposed radial outwards drift. If the plasma temperature is high and the collision frequency is correspondingly low, they can quickly be lost. They are the reason for the unfavourable confinement regime of stellarators at high temperatures, the $1/\nu$-regime. However, if there is a radial electric field the additional $\underline{E} \times \underline{B}$-force leads to an additional poloidal drift that can compensate for the radial outward drift thus reducing the confinement degradation in the $1/\nu$-regime.

Plasmas tend to expand such as to occupy the largest possible volume dV. If the plasma is collisionless then the flux dΦ through a given magnetic flux tube is conserved and the plasma moves to maximise U=dV / dΦ [19,20]. Thus stable plasma operation requires that the maximum of U is in the centre of the plasma and decreases outward. This is called the magnetic well configuration. In toroidal confinement this requirement can only be satisfied in an average sense. The specific volume U of a flux surface can be expressed as $U = \oint \frac{dl}{B}$ (the integration is along the field line and extends to infinity if the surface is not a rational). If U decreases radially outward one has a magnetic well configuration. This is the typical situation in a tokamak.

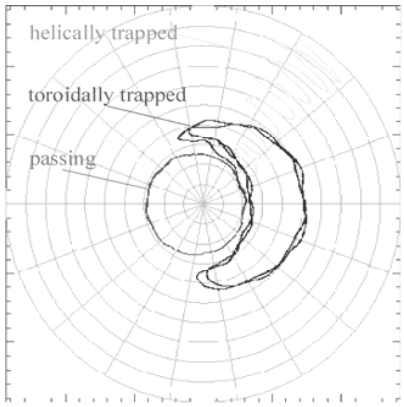

Figure 10 Poloidal cross-section with classes of particle orbits in W7-AS.

TJ-II has been designed to study a wide range of magnetic hill values, in particular it allows to experimentally change from a magnetic well to a magnetic hill configuration.

IV. PLASMA CURRENTS

The vacuum stellarator field confines charged particles. With increased density and temperature of the particles, thus with plasma beta, sizable currents flow in the plasma, that modify the applied magnetic field: They are the Pfirsch-Schlüter current and the bootstrap current. Additional currents can be induced, e.g. ohmically, by absorption of asymmetrically launched electro-magnetic waves or by unbalanced neutral beam injection.

As in a tokamak, plasma equilibrium is established by the force-balance equation: $\underline{j} \times \underline{B} = \nabla p$. This equilibrium also consists of flux surfaces, which are slightly different from the vacuum flux surfaces. They equally fulfil the requirement $\underline{B} \cdot \nabla \Psi = 0$ where ψ is a function that is constant on the flux surface. The diamagnetic current, $j_\perp$, component of $\underline{j}$ balances the pressure gradient. Since this current is not divergence-free an additional current along the field lines is necessary, the Pfirsch-Schlüter current, $j_{P.S.}$, such that $\nabla \cdot \left(\underline{j}_{P.S.} + \underline{j}_\perp \right) = 0$. These two components of the current are indicated in Figure 11.

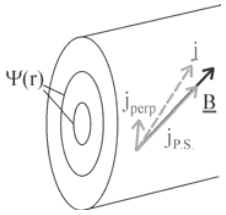

Figure 11 Schematic of the Pfirsch-Schlüter and diamagnetic current component.

In a net-current free stellarator the current filamentsare poloidally closed. This can be seen in Figure 12.

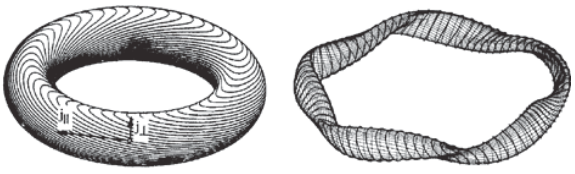

Figure 12 Current filaments on a flux surfaces of a tokamak (left) and of a stellarator (W7-X, right).

Since the Pfirsch-Schlüter current has a large vertical component, this leads to a plasma beta dependent horizontal displacement of the flux surfaces, called Shafranov-Shift Δ_{sh} approximately given by

$$\Delta_{sh} = 4\pi^2 \cdot R \cdot \beta / \iota^2 \quad .$$

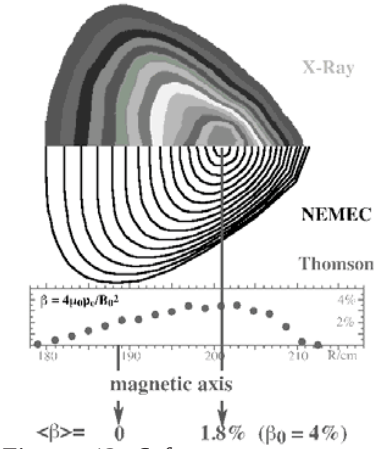

Figure 13 Soft x-ray reconstruction of the plasma temperature profile (upper half), calculated flux surfaces with NEMEC (lower half), plasma beta profile measured with Thomson scattering.

This leads to a limitation of the maximum achievable β since the maximal displacement of the plasma centre at most *a* (the plasma minor radius), thus $\beta_{max} = 4\pi^2 \iota^2 / A$ where A is the aspect ratio, $A = R/a$. This limit, however, can be increased by changing ι or A accordingly or by changing the ratio of $\langle j_\parallel \rangle / \langle j_\perp \rangle$ which is one of the goals in stellarator optimisation [21,22,23]. In the design of the stellarator W7-AS this current ratio was reduced by about a factor of 2 compared to the *l=2*-stellarator W7-A. Experimentally, the resulting Shafranov-Shift can be inferred directly from the actual displacement of the hot plasma centres observed with soft X-ray tomography [23] as shown in Figure 13.

Figure 14 shows the measured plasma centre displacement for various values of the plasma beta as inferred from soft x-ray data for various values of plasma beta. The calculated values for a l=2 stellarator are shown for comparison. This demonstrates that the optimisation goal of reducing the Shafranov shift in W7-AS was achieved. The displacement of the plasma can also be deduced from measuring the vertical flux associated with the Pfirsch-Schlüter currents [25].

Similar to a tokamak plasma also a stellarator plasma generates a toroidal current as a result of the plasma density gradient and the friction between trapped and untrapped particles. Figure 15 sketches the orbit of a toroidally trapped particle. Superposed on the banana-orbit motion is a precession in toroidal direction (shown left). On the r.h.s. the orbit is shown in its poloidal projection. If there is a density gradient then there is a local toroidal flux of particles. Since they are trapped there no toroidal net current is associated with that. However, fractional drag with passing particles leads to a toroidal net current, the bootstrap current.

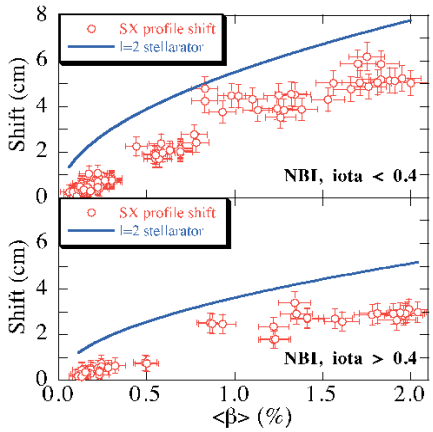

Figure 14 Measured Shafranov shift versus volume averaged plasma beta.

As was pointed out before in a stellarator particles can be helically trapped. Their drift direction is opposite to toroidally trapped particles due to the sign change of $\underline{B}\times\underline{\nabla}B$. This is illustrated in Figure 16 for the special case of a true helical stellarator. Thus the associated bootstrap current has the opposite sign of the current caused by toroidally trapped particles.

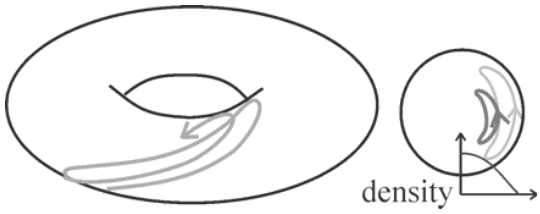

Figure 15 Perspective and poloidal projection of toroidally trapped particles. Density gradient causes a toroidal particle flux.

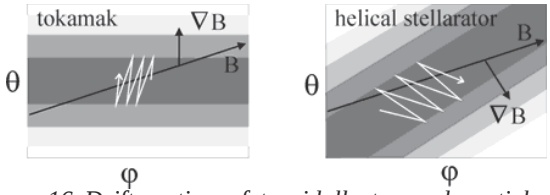

Figure 16 Drift motion of toroidally trapped particle in tokamak and helically trapped particle in a stellarator.

The bootstrap current reduces the externally applied rotational transform whereas the bootstrap current associated with toroidally trapped particles increases the rotational transform. Since it is undesirable to have the rotational transform being modified by the plasma pressure one can minimise the bootstrap current by an optimisation procedure: by balancing the toroidal and helical component of the field against each other. Any residual bootstrap current can be easily measured in a stellarator plasma since it is not necessary to separate out the (large) inductive plasma current as in a tokamak plasma. Figure 17 shows the measured and calculated values on ATF where by changing the value of the quadruple moment of the magnetic field one could change the ratio of helically and toroidally trapped particles [26] and thus the sign of the bootstrap current. The bootstrap current was measured with a Rogowski coil.

Perfect cancellation of the bootstrap current for all values of plasma beta and magnetic configurations is not possible. Therefore it is important to have means to compensate for the residual bootstrap current. This can be done by installing an Ohmic transformer (like in a tokamak) and inducing a compensation current in the plasma. But even if the total current is compensated it is locally not compensated since the ohmic current density profile peaks in the plasma center where the electron temperature is highest and the plasma resistivity is lowest whereas the bootstrap current peaks off-axis where the density gradient is highest. This can lead to different ι-profiles for constant edge ι(a) and might have degrading effects on plasma confinement. Another means is driving a current non-inductively by launching electromagnetic waves in preferentially one toroidal direction. For example, in electron cyclotron heating (ECH) the direction of the wave propagation can be steered with a mirror. Finally a current can also be driven in a plasma by heating with tangential, unbalanced neutral beam injection. For example, W7-X that is optimised for minimal the bootstrap current still requires up to 50 kA of externally driven toroidal plasma current driven by external means for compensation.

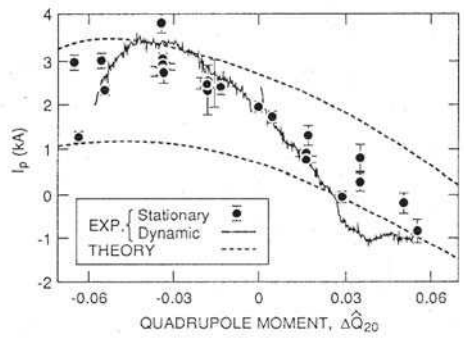

Figure 17 Bootstrap current in ATF.

V. PLASMA CONFINEMENT

This section describes how the different parameters of the vacuum magnetic field, such as the rotational transform, the shear and the magnetic well, influence plasma.

Off all magnetic flux surfaces those that have a rotational transform ι are singular. They are particular susceptible to small field perturbations in which case they form islands that short-circuit the inner plasma region with the outer region. Thus the plasma confinement is deteriorated. Strong shear inhibits the formation of islands. However, strong shear in a plasma also means that the ι-profile crosses a number of those "low order rational surfaces". Higher order rational surfaces are not important

since the large number of necessary toroidal and poloidal rotations renders other effects more important which prevent the creation of islands. The fractions made up of low integers are not equally densely spaced, rather regions around the simplest fractions, like 1/ 2, are void of higher fractions. The low shear stellarators show the highest confinement times in these regions. This is shown in Figure 18 where the plasma energy is plotted versus ι*(a)* over a wide experimental range of the rotational transform on W7-AS [15]. Near the low order rationals the energy shows pronounced maxima. In contrast, high shear stellarators do not show such a dependence.

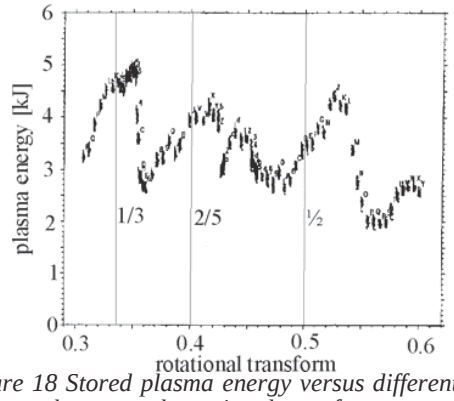

Figure 18 Stored plasma energy versus different values of the external rotational transform.

The dependence of the stored energy on the combination of ι and magnetic shear can be understood in more detail. By inducing a current in the plasma and changing the magnetic field configuration accordingly one can change the ι-profile while keeping the edge value ι*(a)* constant. In Figure 19 calculated ι-profiles are shown with approximately the same ι(a) but different profiles [27]. The horizontal lines indicate lower order rationals. The discharges with either a ι(r)-profile in the rational free zone or with strong shear (due to the induced current) have similar stored energies. Their ι-profiles are shown with solid lines. The stored energy belonging to the discharge that has a ι-profile neither in the rational-free zone nor with strong shear (shown with dashed lines) is only half as large than the others. Therefore in low shear devices like W7-AS and W7-X it is necessary to keep the iota-profile in a resonance-free region or add sufficient shear with an additional current to obtain optimal confinement.

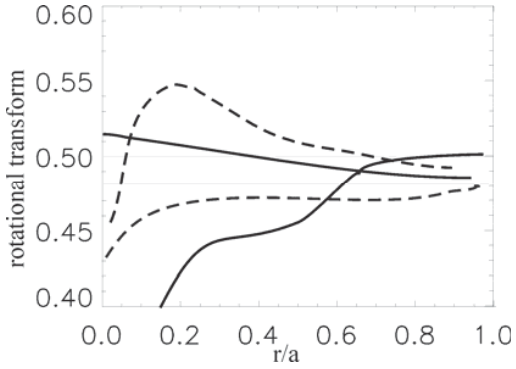

Figure 19 iota profiles for good confinement (solid) and poor confinement (dashed).

The importance of the magnetic well is investigated in TJ-II. By changing the magnetic configuration from a magnetic well near the plasma edge to a magnetic hill the relative plasma density fluctuation level at the plasma edge doubled [28]. Whether this increased level of plasma density fluctuations is caused by pressure driven instabilities and whether this leads to a degraded plasma confinement is still under investigation.

VI. NEOCLASSICAL TRANSPORT

Neo-classical transport theory is the calculation of the transport coefficients (particle, energy, momentum) based on the particle drift orbits. The transport is calculated with a diffusion equation (assuming a random walk of the particles away from its flux surface) with a diffusion coefficient χ given by $\chi = \Delta r^2 / \tau_{coll}$, where Δr is the step size of the particle between two collisions and τ_{coll} is the time between two collisions. When collisions are important and the mean free path of the particles is short, the neo-classical predictions for stellarators and tokamaks are similar. Thus a stellarator exhibits a Pfirsch-Schlüter regime and a plateau regime corresponding to a tokamak. At even lower collision frequencies and thus longer mean free path lengths the transport coefficients show an increase inversely proportional to the collision frequency, called the $1/\nu$-regime. This behavior is due to helically trapped particles. As was shown before helically trapped particles are localized in a small poloidal range. Their radial outward drift is fast. Therefore if the collision frequency is low, particles that are helically trapped increase the radial transport. This behavior is shown in Figure 20 for W7-AS.

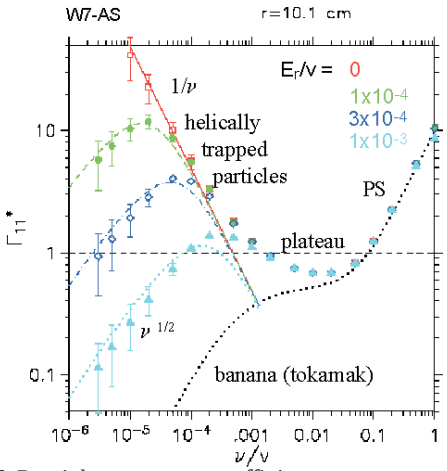

Figure 20 Particle transport coefficient versus normalised collision frequency.

With this $1/\nu$-behaviour a stellarator would be unacceptable for a reactor because the energy and particle loss in the temperature regime where the reactor operates would be too large. An improvement of the neo-classical

confinement can be obtained either by optimising the magnetic field and limiting the number of helically trapped particles or by an additional radial electric field that limits the excursions of the helically trapped particles due to an additional $\underline{E}\times\underline{B}$ poloidal rotation [29]. With the radial electric field one obtains a region of a reduced transport coefficient that has a $\sqrt{\nu}$ -dependence. Figure 20 shows the reduction for different values of the radial electric field, however, the values for W7-AS are still above those of an equivalent tokamak. In tokamaks there is no dependence of the transport coefficients on the radial electric field as long as the banana orbits still exist.

The electric field adjusts itself self-consistently according to the requirement of ambipolarity whereby the outward particle fluxes of electrons Γ_e and ions Γ_i are equal. Since the transport coefficients depend on E_r even multiple solutions ("roots") of this condition are possible. In most discharges the "ion root" is observed with a rather small negative electric field and comparable electron and ion temperatures. With strong central electron heating it is also possible to obtain the "electron root" in the centre of the plasma with positive electric field and $T_e >> T_i$. In Figure 21 l.h.s. the radial profile of the radial electric field is shown [27] for W7-AS. The lines are neo-classical calculations that at some locations have the two "roots". In Figure 21 r.h.s. the heat transport coefficient is calculated from the two roots and compared with the experimentally determined coefficient. Near the centre experimental and neo-classical values approximately agree with each other. Near the plasma edge the experimental values are much larger than the neo-classical values. Because of the small values of the transport coefficient these discharges have record electron temperatures [30]. The enhancement of the measured transport over the neo-classical transport is called anomalous transport and is particularly pronounced for electrons. Similar results are reported from CHS [31].

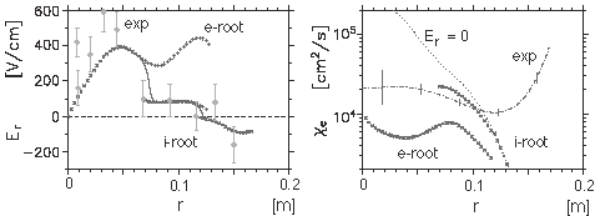

Figure 21 Calculated and measured electric field and calculated and measured electron heat transport coefficient.

The highest ion temperatures in W7-AS were obtained in discharges with a combination of electron cyclotron resonance heating and neutral beam injection [32,33]. These discharges were characterised by neo-classical electron and ion transport in the plasma centre up to 75% of the plasma radius and strong anomalous transport in the plasma edge region.

VII. TOWARDS A STELLARATOR REACTOR

In recent years the focus of stellarator research has become dominated by the demands of a fusion reactor. These studies include the investigation of

- parametric dependence of the plasma confinement on global quantities with the goal of extrapolating to the necessary size of a stellarator fusion reactor,
- high beta discharges and the search for instabilities that might limit the maximum achievable plasma beta,
- in-vessel components suitable to withstand high heat load and simultaneously causing little increase of impurity concentration in the plasma,
- long pulse discharges to verify the steady-state viability,
- non-inductive current drive to balance the internally generated plasma currents.

The plasma confinement properties of different helical devices are compared with one another by fitting the measured energy confinement time to a product of global quantities of minor radius a, major radius R, absorbed heating power P, on-axis magnetic field B, volume-averaged density n and edge rotational transform ι(a) with to be determined exponents. The energy confinement time τ_E is calculated from the measured stored plasma energy and heating power according to $\tau_E \equiv W/\left(P - dW/dt\right)$. This resulted in the International Stellarator Scaling ISS95 [34] given by

$$\tau_E \propto a^{2.21} \cdot R^{0.65} \cdot P^{-0.59} \cdot n^{0.51} \cdot B^{0.83} \cdot \iota^{0.4} .$$

The scaling is well fitted by all helical devices. Note the positive dependence on minor and major axis. W7-AS and LHD have a proportionality factor that is between 1.5 and 2 higher than the scaling. This can be seen in Figure 22 where the measured energy confinement time is plotted versus the predicted value from ISS95.

In addition, values from tokamak L-mode discharges are shown that approximately follow the same scaling. The highest values belong to JET. In tokamaks, typically a factor of 2 improvement is obtained in H-mode discharges. The parametric dependence of tokamaks and stellarators is similar except that tokamaks do not show a positive dependence on density and stellarators do not show a dependence on particle mass of the plasma. Extrapolation based on this scaling is used in order to determine the required size of a reactor. Thus obtained dimensions (R=20m, a=2m) are considered feasible (see Section VIII).

An economically attractive reactor has to operate at the highest plasma beta possible since the magnetic field coils amount to about a third of the reactor investment costs. Therefore the optimisation process of the stellarator magnetic fields includes the plasma stability against pressure driven instabilities. For example, W7-X has been optimised for maximum average beta value of 5%. In W7-AS and LHD the maximum beta values were calculated to be about 2%. In both devices the predicted maximum beta

values have been surpassed in experiments and up to now the maximum achievable b has been limited by the available heating power and not by deleterious pressure driven instabilities [35,36,36].

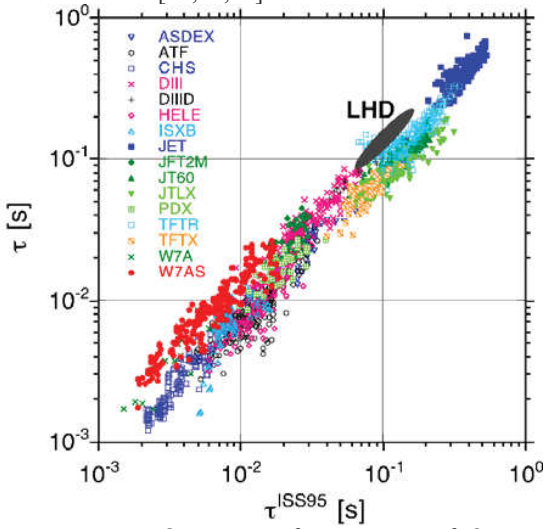

Figure 22 Measured energy confinement time of plasmas in helical devices and L-mode tokamak discharges versus international stellarator scaling ISS95.

Stellarators are inherently capable of steady-state operation since plasma confinement does not require a constantly driven toroidal plasma current LHD and W7-X are equipped with super-conducting coils. It also requires plasma heating methods capable of steady-state operation. Appropriate sources for neutral beam injection and electromagnetic wave generation are being developed at present. In ATF a one-hour discharge has been achieved at small power level with electron cyclotron heating and low values of magnetic field and plasma density [38]. In LHD plasma discharges at higher power levels and magnetic fields have reached a duration of several minutes. An example for a plasma shot over longer than a minute is shown in Figure 23 [39,39].

Stellarators and tokamaks need to keep impurities that are released by wall sputtering from entering the plasma and need to keep the heat load on any surface low. In a tokamak this is done adding additional coils to generate an X-point. Fanning out the plasma near there and directing it at acute angles on target plates, the divertor plates, it is possible to keep the core plasma well separated from the edge region. The magnetic surface that passes through the X-point becomes the last closed flux surface. Thus the magnetic field lines that intersect the target plates have no direct connection to the interior plasma. In a stellarator it is not possible to introduce additional X-points, however, the natural islands (compare Figure 24 l.h.s.) already provide such X-points. In an island divertor these islands are intersected with high heat load resilient target plates. Thus a similar separation of plasma-target interaction zone and main plasma as in a tokamak is achieved. It is also possible to intersect the helical islands that exist outside of a heliotron. This has been done on LHD where graphite tiles have been installed that intersect the helical plasma fans (compare Figure 24 r.h.s.). This reduced the iron impurity influx and led to improved plasma performance [39].

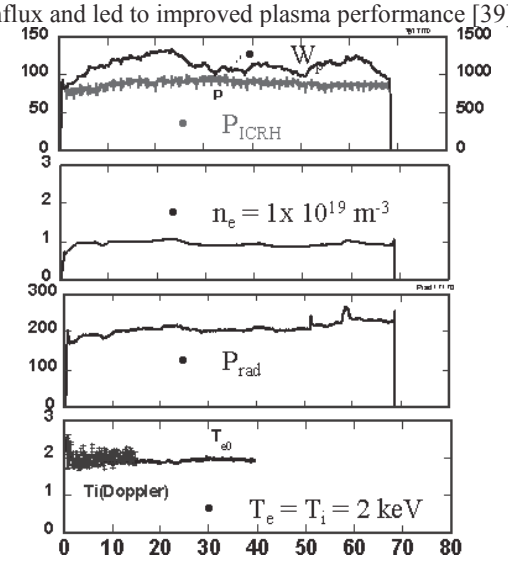

Figure 23 Long pulse discharge done with ion cyclotron resonance heating on LHD

On W7-AS an island divertor has recently been installed. In contrast to a tokamak it consists of 5 × 2 modules located at isomorphic positions in the vessel. Figure 24 shows a picture of one module before installation. Each module consists of two graphite target plates separated by a small pumping region that intersect the islands and baffles that shield the back side of the divertor module from the plasma region and allow for additional gas pumping.

The first results obtained with this divertor are encouraging [17,43]. It facilitated plasma operation at high densities (line-averaged density $>3\times10^{20}\,m^{-3}$) under steady-state conditions for the longest plasma duration possible in the device. The plasma edge temperature in the vicinity of the target plates could be reduced to values of about 10 eV. At this temperature the plasma ions start to recombine and high radiation loss occurs due to partially ionised carbon (partial detachment). This isotropic radiation reduces the heat load on the target plates and therefore also the sputtering of target material. Thus the radiation profile of the plasma was dominated by the radiation from the plasma edge. In addition, it was found that the confinement time of artificially injected impurities (aluminum) decreased in these high density scenarios which is very encouraging for reactor operation. Finally, the density in these discharges was sufficiently high to heat the plasma centrally with electron cyclotron resonance heating overcoming the usual plasma density cut-off for wave propagation by invoking a mode conversion of the ordinary plasma wave into an electron Bernstein wave [30]. The same type of divertor will also be used for W7-X.

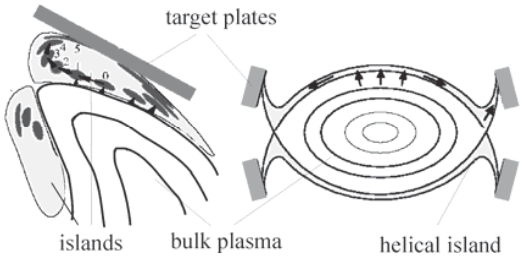

Figure 24 Schematic of the island divertor of W7-AS and of the helical divertor of LHD.

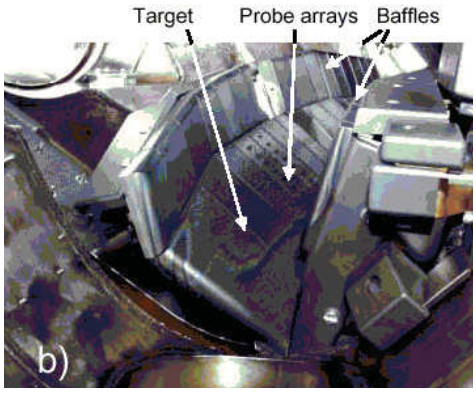

Figure 25 Picture of one module of the island divertor of W7-AS.

Studies investigate the stellarator reactor properties based on the concept of LHD and W7-X [19,41]. Based on the experimental confinement time scaling of W7-AS a helias reactor (optimisation similar to W7-X) that yields a fusion power of 3000 MW has a major radius of 18m and a minor radius of about 2m. The field at the coils is sufficiently low to allow the use of conventional NbTi super-conductors. The total weight of the super-conducting coils will be less than half of that for ITER which will significantly reduce the costs of the device. However, the manufacturing costs of the non-planar coils will be higher. The larger aspect ratio than a tokamak and therefore the increased area of the vessel reduces the neutron wall loading such that blanket segments probably need to be replaced less often than in a comparable tokamak reactor.

VIII. PHYSICS CHALLENGES OF THE STELLARATOR CONCEPT

In order to feel confident about proposing the stellarator as a viable fusion reactor concept a number of physics challenges still have to be overcome or their proposed remedies have to be demonstrated. The neo-classical transport in the reactor regime has to be reduced to levels acceptable in a reactor. This can be done by further optimisation of the magnetic field in particular by generating magnetic fields that have quasi-symmetries (quasi-helical, quasi-axial, quasi-omnigeneous) from the particle point of view or by enhancing the radial particle flux of one species to drive a radial electric field. Experiments are in planning or have already been build that will test these approaches. The viability of the island divertor has to be experimentally demonstrated. The current profile control with ECH or tangential neutral beam for bootstrap current compensation has to be tested in high density situations. Whether there is an experimental limit to the maximum achievable plasma beta imposed by magnetohydrodynamic events still has to be investigated. Up to now no universal features have been identified that account for limitations of the maximum achievable energy. Central particle refuelling could be a problem [42] but might be accomplished with negative neutral beam injection. Finally high α-particle confinement at high energies and simultaneously low confinement at thermal energies for helium ash removal still have to be investigated.

IX BUILDING WENDELSTEIN 7-X

A number of the issues raised in the previous section are planned to be addressed in the stellarator experiment Wendelstein 7-X (W7-X). This experiment is presently being built at the Max-Planck Institute for Plasma Physics in Greifswald. Completion of assembly is planned for end of 2015 and start of commissioning for beginning of 2016.

The goals of W7-X have been chosen to be reactor relevant [45]. Thus it is to achieve quasi-steady state operation at temperatures in excess of 5 keV and densities on the order of 10 20 m-3, to reach plasma equilibrium with an average beta of 5%, to control plasma density and its impurity content. Ignition is not one of the goals, thus the device will not be operated with a tritium, deuterium mixture. Plasma experiments, therefore have to be done with external plasma heating.

The structure of the magnetic field is decisive for the

energy confinement time of stellarators even though also for these devices anomalous transport is a dominant factor. Therefore the structure of the magnetic field has been chosen such that simultaneously a number of criteria are met [45]:

(1) Magnetic surfaces with a corresponding iota profile that avoid low order resonances to limit the effect of islands.
(2) A small Shafranov shift to yield a high beta limit and to allow installation of an island divertor.
(3) Good magneto hydrodynamic stability via a magnetic well to achieve a high plasma beta.
(4) Reduced neoclassical transport in the 1/v regime.
(5) Small bootstrap current to avoid changing the iota profile to create low resonance islands
(6) Good modular coil feasibility (only modular coils allow generation of the magnetic field that meets the criteria (1)-(5)).

The magnetic field that meets these requirements is called to have a quasi-isodynamic property [46].

The basic parameters of W7-X to generate such a magnetic field and to achieve the experimental goals mentioned above are: Major average radius 5.5m, minor average radius 0.5 m, a magnetic field of up to 3 T on axis, 10 MW cw plasma heating with ECRH for up to 30 minutes, up to 20 MW of pulsed (10 sec) NBI heating.

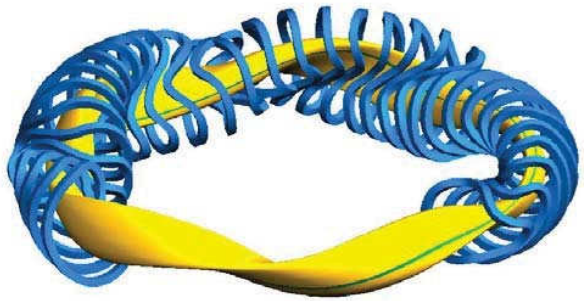

Figure 26 Simplified non-planar coils of 3.5 modules of W7-X and the lcfs of the plasma

The magnetic field is generated a set of 50 modular superconducting coils of 5 different types supplemented by a set of 20 superconducting planar coils of two types for added experimental flexibility arranged in a five-fold symmetry (Fig. 26). The coils are wound of NbTi strands in an aluminium cable with in-conduit He cooling that are placed in a stainless steel housing. Coils of the same type are electrically connected in series and powered by an independent power supply. All coils are bolted to a support structure that forms an inner ring in the torus. Additional support elements are added between neighbouring coils. All coils and coil housings are individually supplied with liquid helium.

All the magnets, the support structures and supply lines are lined in a toroidal, vacuum tight double shell structure, called the cryostat, whose inner wall is the plasma vessel. All inside surfaces of the cryostat are insulated against thermal radiation by multilayer aluminium coated capton foils under a thermal shield helium cooled to 80 K.

The plasma vessel and its 254 ports have to be protected from convective, radiation and fast particle plasma losses while sources for plasma impurities have to be kept sufficiently small. A toroidally extended island divertor is installed at ten symmetric locations in the plasma vessel that is designed to withstand the convective losses of up to 10 MW/m2. Its plasma facing elements consists of CFC material that is brazed on an actively water-cooled support structure. The area close to the divertor can be actively pumped with cryo pumps to reduce the effects of recycling and impurity generation on the plasma. Additional control coils that can be operated with a AC current can diffuse the magnetic field lines to reduce the heat load. Areas of the plasma with reduced convective losses of up to 500 kW/m2 are covered with graphite tiles that are clamped onto a water-cooled support structure. Areas where no convective losses are expected including the inside walls of the 254 ports are covered with water cooled stainless steel sheets. The cooling circuits occupy about 120 of the 254 ports. The remainder is used for plasma heating and diagnostics. A schematic cut-open view of the basic device is shown in Fig. 27.

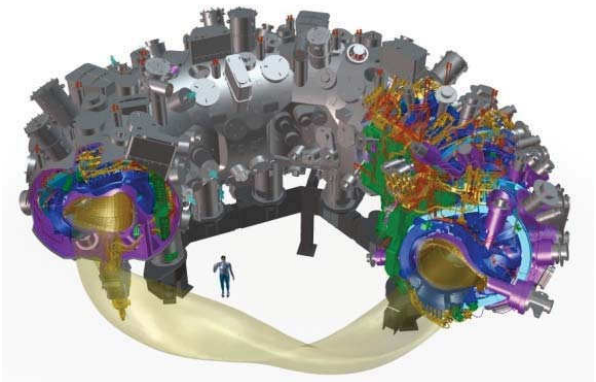

Figure 27 Schematic, cut-open view of the basic device of Wendelstein 7-X.

The plasma heating systems consists of 10 gyrotrons at 140 GHz with a nominal power of 1 MW each during steady-stte operation for ECRH heating, predominately 2nd X mode heating. The power is transported into the torus hall with optical transmission and directed into the plasma using steerable mirrors thus facilitating current drive and also advanced heating methods. Further heating for high beat experiments and studies of particle confinement is provided by 2 NBI injectors with 4 sources each for pulsed 2.5 MW injection at up to 90 keV D. Eventually, also a 4 MW ICRH system will be installed for high beta experiments and further studies with fast hydrogen ions.

The diagnostic systems are being prepared to allow full characterization of the plasmas. A Thomson scattering system with 50 channels will measure electron temperature and density every 50 msec. A dispersion interferometer system with 5 channels will measure the line integrated

electron density continuously. An ECE radiometer will measure the electron temperature profiles at 24 different locations. A test neutral beam injector system will measure the ion temperature at three adaptable locations. A bolometer system to measure the 2 D shape of the flux surfaces at finite beta experiments. Magnetic diagnostics measure the diamagnetic energy, the plasma current profile and magneto-hydrodynamic fluctuations.

The assembly of the device is organized by identifying sub components that can be pre-assembled to reduce the number of required assembly steps in the torus hall. To that purpose all coils of one half module that corresponds to a 36° segment of the device where first mounted onto the appropriate sector of the plasma vessel and attached to the sector of the central support structure before mounted to the neighboring half module to form one complete module. Cryo lines and the bus lines for the electrical coil connections were installed if possible. This sub-assembly were then lowered into the lower half shell of the outer vessel, placed on the machine base into the torus hall, before one module was then completed by welding the upper shell of the outer vessel on top. Thus subsequently the five modules were placed onto the machine base in the torus hall where the attachments of the segments of the central support structure to its neighbours, the cryo and bus lines, the thermal insulation, plasma vessel and the outer vessel was done. Since the overall required accuracy of the location of the current paths of the coils has to be on the order of a few millimetres, great care was taken to ensure that during the subsequent assembly steps there was no accumulation of an intolerable large error. The 254 ports and the current leads that provide feed throughs for the coil current are installed then. The view of the experimental hall after four modules have been installed (2012) is shown in Fig. 28.

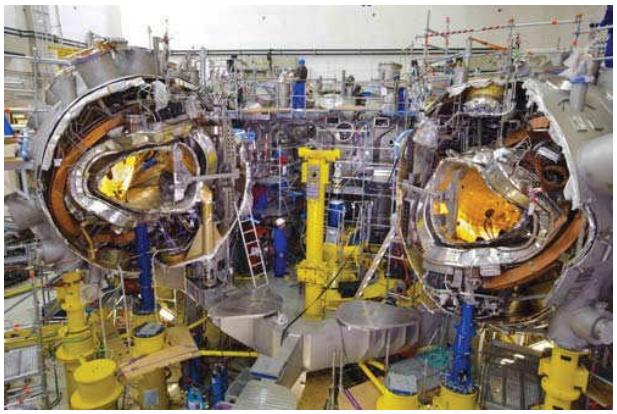

Figure 28 View of the basic device in the experimental hall when four of the five modules were installed.

The installation of the components inside the plasma vessel is done in two steps corresponding to two phases of operation. In the first phase when the total injected energy per plasma discharge will be limited to 50 MJ uncooled divertor units will be installed together with a subset of the wall panels and graphite protections. For a second phase of operation these divertor units are replaced with the completely water cooled divertor units and all other protective elements and diagnostics will be installed. Presently, as of summer 2013, the plasma vessel components for the operational phase 1 are being installed.

In addition to the device itself, a number of additional components (e.g. diagnostics, heating systems, peripheral supply lines, support structures) have to be placed in the experimental hall. Due to the limited space and the need for simultaneous development the design and the layout of these components have to be done following the principles of concurrent engineering. To that purpose a reference CAD model set is updated daily that describes the present sate and maturity of the design of the various components and configuration management tools are applied throughout. The present design of the torus hall is shown in Fig. 28.

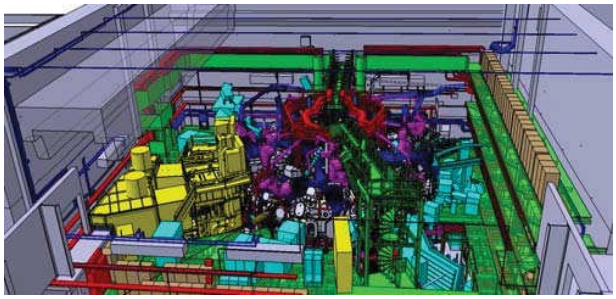

Figure 29: CAD view of the experimental hall with the basic device (grey), heating systems (yellow), cooling water lines (blue), cable trays (red), support structures (green), vacuum systems (magenda), cubicles (brown), diagnostics (light blue) diverse infrastructure elements (light grey).

At present plans are being developed to commission the about 50 main systems for operation. First each system needs to be provided with the required means for operation. Thus these supply systems have first to be commissioned on their own. Each system is then put into local operation. Then the complete system of W7-X is sequentially put into operation. In order to save time commissioning processes have been parallelized wherever possible, certain commissioning processes even run in parallel to remaining assembly processes. Care is been taken to check for all logical interdependencies that have to be taken into account. It is planned to put the cryostat under vacuum first before evacuating the plasma vessel. During the subsequent cool-down of the cryostat the deformation of the magnet system is being measured. After the coils have been successfully energized the accuracy of the magnetic field is then measured. Should magnetic field errors be detected that cannot be tolerated the trim coils will be put into operation to correct for them. A short experimental campaign to provide a first check of the ECRH heating system and principle diagnostics will then conclude this first operational phase in the beginning of 2015. After that campaign the assembly of remaining components of the plasma vessel will resume to then start the first experimental exploration of W7-X late in 2015.

REFERENCES

1. M. Van Schoor, “Fusion Machines”, these proceedings.
2. Jaspers, “Thermonuclear Burn Criteria”, these proceedings.
3. L. Spitzer, Phys. Fluids 1, 253 (1958).
4. A. Iiyoshi et al., Nucl. Fusion 39, 1245 (1999).
5. G. Grieger, J. Plasma Fusion Res., (1998).
6. D.T. Anderson et al., J. Plasma Fusion Res. SERIES, Vol. 1 (1998).
7. B.A. Carreras et al., Nuclear Fusion 28, 1613 (1988).
8. G. Grieger et a., Nuclear Fusion 25, 1231 (1985).
9. J.I. Shohet in Fusion (Ed. E. Teller) Vol. I, 243, Academic Press, Cambridge 1980.
10. C. Alejaldre et al., Plasma Physics Control. Fusion 41, 539 (1999).
11. J. Nührenberg et al., Phys. Lett. A 129, 113 (1988).
12. D.A. Spong, 18th Fusion Energy Conf. Proc. 2000.
13. E. Ascasibar, J. Plasma Fus. Res., 1, 183 (1998).
14. Komori, Stell. News 58, 1 (1998).
15. R. Jaenicke et al., Nucl. Fusion 33, 687 (1993).
16. De Blank, “Plasma Equilibrium in Tokamaks”, these proceedings.
17. P. Grigull et al., Plas. Phys. Cont. Fus. 43, A175, (2001)
18. H.J. de Blank, “Guiding Center Motion”, these proceedings.
19. M. Wakatani, “Stellarator and Heliotron Devices”, Oxford University Press, 1998.
20. K. Miyamoto, “Plasma Physics for Nuclear Fusion”, MIT Press, 1989.
21. J. Nührenberg et al., Trans. Fusion Technology 27, 71 (1995).
22. G. Grieger et al., Physics of Fluids B 4, 2081 (1992).
23. H. Wobig, Plasma Physics and Contr. Fusion 35, 903 (1993).
24. Weller et al., Plasma Phys. And Contr. Fusion 11, 1559 (1991).
25. H. Renner et al., Controlled Fusion and Plasma Physics, Proc. 19th European Conf., Innsbruck, 1992, Vol. 16C, Part I, 501.
26. M. Murakami, Phys. Rev. Lett. 66, 707 (1991).
27. R. Brakel et al., Plasma Phys. Control. Fusion 39, B273 (1997).
28. C. Alejaldre et al., 18th Fusion Energy Conf. Proc., 2000.
29. H. Maassberg et al., Plas. Phys. Contr. Fus. 35, B319 (1993).
30. H. Laqua et al., Phys. Rev. Lett. 78, 3467 (1997).
31. H. Idei et al., Phys. Rev. Lett. 71, 2220 (1993).
32. R. Jaenicke et al., Plas. Phys Contr. Fus. 37A, 163 (1995).
33. J. Baldzuhn et al., Plasma Physics Control. Fusion 40, 967 (1998).
34. U. Stroth et al., Nucl. Fusion 36, 106 (1996).
35. M. Fujiwara et al., 18th Fusion Energy Conf. Proc. 2000.
36. R. Jaenicke et al., 18th Fusion Energy Conf. Proc. 2000.
37. Weller et al, Phys. Plas., 8, 931, (2001).
38. T.C. Jernigan et al., Phys. Plas., 2, 2435, (1995).
39. R. Kumazawa et al., Phys. Plas., 8, 2139 (2001). LHD, Stell. News 62 (1999).
40. Komori et al., Phys. Plas., 8, 2002, (2001)
41. C.D. Beidler et al., 18th Fusion Energy Conf. Proc. 2000.
42. H. Maassberg et al., Plasma Physics Control. Fusion 41, 1135 (1999).
43. M. Hirsch et al., Plasma Phys. Control. Fusion **50** (2008)
44. H. Wobig et al., „Nuclear Energy“, Vol. 3B, chapter 7, Springer, Berlin, 2005, p. 418.
45. C. Beidler et al. Fus. Tech., 17, 11, (1990)
46. C. Beidler et al., Nucl. Fusion 51, 1 (2011)